

TESTING THE UNIVERSALITY OF THE STELLAR IMF WITH *CHANDRA* AND *HST*

D. A. COULTER,^{1,2} B. D. LEHMER,³ R. T. EUFRASIO,^{2,3} A. KUNDU,⁴ T. MACCARONE,⁵ M. PEACOCK,⁶ A. E. HORNSCHEMEIER,²
A. BASU-ZYCH,² A. H. GONZALEZ,⁷ C. MARASTON,⁸ & S. E. ZEPF⁵

Draft version November 10, 2018

ABSTRACT

The stellar initial mass function (IMF), which is often assumed to be universal across unresolved stellar populations, has recently been suggested to be “bottom-heavy” for massive ellipticals. In these galaxies, the prevalence of gravity-sensitive absorption lines (e.g. Na I and Ca II) in their near-IR spectra implies an excess of low-mass ($m \lesssim 0.5 M_{\odot}$) stars over that expected from a canonical IMF observed in low-mass ellipticals. A direct extrapolation of such a bottom-heavy IMF to high stellar masses ($m \gtrsim 8 M_{\odot}$) would lead to a corresponding deficit of neutron stars and black holes, and therefore of low-mass X-ray binaries (LMXBs), per unit near-IR luminosity in these galaxies. Peacock et al. (2014) searched for evidence of this trend and found that the observed number of LMXBs per unit K -band luminosity (N/L_K) was nearly constant. We extend this work using new and archival *Chandra X-ray Observatory (Chandra)* and *Hubble Space Telescope (HST)* observations of seven low-mass ellipticals where N/L_K is expected to be the largest and compare these data with a variety of IMF models to test which are consistent with the observed N/L_K . We reproduce the result of Peacock et al. (2014), strengthening the constraint that the slope of the IMF at $m \gtrsim 8 M_{\odot}$ must be consistent with a Kroupa-like IMF. We construct an IMF model that is a linear combination of a Milky Way-like IMF and a broken power-law IMF, with a steep slope ($\alpha_1 = 3.84$) for stars $< 0.5 M_{\odot}$ (as suggested by near-IR indices), and that flattens out ($\alpha_2 = 2.14$) for stars $> 0.5 M_{\odot}$, and discuss its wider ramifications and limitations.

Subject headings: X-rays: binaries — galaxies: elliptical — initial mass function

1. INTRODUCTION

Understanding the stellar initial mass function (IMF) has major implications for a variety of astrophysical problems. The IMF plays a central role in converting the observed properties of galaxies (e.g., luminosity and color) into physically meaningful quantities like stellar mass and star-formation rate. An assumed universality of the IMF has contributed to our current observational-based paradigm of how galaxies formed and evolved throughout the history of the Universe, what fraction of the Universe’s mass is tied up in stellar baryons, and the number of compact objects in the Universe. A clear understanding of the form and universality of the IMF in external galaxies is therefore a central goal in modern astrophysics (see, e.g., Bastian et al. 2010 for a review).

In recent years, there has been mounting evidence indicating that the stellar IMFs for elliptical galaxies vary with galaxy mass. For example, Cappellari et al. (2012) used detailed dynamical models and two-dimensional stellar kinematic maps of 260 early-type galaxies from the ATLAS^{3D} project to show that the mass-to-light ratios (M/L) for elliptical galaxies increase with increasing stellar velocity dispersion, σ , consistent with a scenario where the IMF changes with galaxy mass. Such a finding has been independently noted in galaxy lensing measurements of M/L for a variety of σ (e.g., Auger et al. 2010; Treu et al. 2010). Specifically, these

findings indicate that relatively low-mass, early-type galaxies ($\sigma \lesssim 100 \text{ km s}^{-1}$) have M/L values consistent with standard Milky Way-like IMFs (Kroupa 2001; Chabrier 2003). However, relatively massive ellipticals ($\sigma \approx 300 \text{ km s}^{-1}$) have mass-to-light ratios (M/L) that are larger than those predicted from standard IMFs, and can be consistent with either “bottom-heavy” IMFs ($\alpha \approx 2.8$, yielding more low-mass stars with higher M/L) or “top-heavy” IMFs ($\alpha \approx 1.5$, yielding more remnants with lower luminosities; Cappellari et al. 2012).

Van Dokkum & Conroy (2010, 2011, 2012) and Conroy & van Dokkum (2012) showed that the spectra of massive ellipticals have strong Na I and Ca II absorption features that are indicative of a large population of very low-mass stars ($\lesssim 0.3 M_{\odot}$; Saglia et al. 2002), favoring the bottom-heavy IMF interpretation for these galaxies. These features had been known for quite some time (see, e.g. Hardy & Couture 1988; Cenarro et al. 2003), but higher-quality data and spectral stellar synthesis modeling in recent years has given more confidence to the interpretation that the stellar IMFs in these galaxies are likely to be bottom-heavy and consistent with $\alpha \approx 2.8$.

Despite the above evidence for a bottom-heavy IMF in massive ellipticals, some inconsistencies remain. For example, Smith and Lucey (2013), found that a bottom-heavy IMF is incompatible with the stellar mass obtained via strong lensing, for a ($\sigma \approx 300 \text{ km s}^{-1}$) galaxy. Smith (2014) has also shown, intriguingly, that there is no correlation between results based on near-IR indices and on dynamics, on a galaxy-by-galaxy basis. Additionally, Weidner et al. (2013) showed that a time-invariant and bottom-heavy IMF was incompatible with the observed chemical enrichment of massive ellipticals, and underpredicted the number of stellar remnants (in the form of LMXBs) observed in globular clusters (GCs). To resolve this, they proposed a time-dependent IMF model that would evolve from a top-heavy to bottom-heavy form. In this scenario, the

¹ University of California Santa Cruz, Santa Cruz, CA 95064, USA

² NASA Goddard Space Flight Center, Code 662, Greenbelt, MD 20771, USA

³ Department of Physics, University of Arkansas, 226 Physics Building, 835 West Dickson Street, Fayetteville, AR 72701, USA

⁴ Eureka Scientific, Oakland, CA 94602, USA

⁵ Texas Tech University, Lubbock, TX 79409, USA

⁶ Michigan State University, East Lansing, MI 48824, USA

⁷ University of Florida, Gainesville, FL 32611, USA

⁸ University of Portsmouth, Portsmouth, United Kingdom

Table 1
Properties of Low-Mass Elliptical Galaxy Sample

Source Name (1)	D (Mpc) (2)	σ (km s ⁻¹) (3)	a (arcmin) (4)	b (arcmin) (5)	$\log L_K$ (log $L_{K,\odot}$) (6)	N_H (10 ²⁰ cm ⁻²) (7)	HST ACS Data (Blue Filter) (8)	(Red Filter) (9)	t_{exp} (ks) (10)	N_{LMXB} (field) (11)	$N_{X,GC}$ (GCs) (12)	$N_{X,bkg}$ (Background) (13)
NGC 4339	16.0	100.0	1.3	1.1	10.3 [†]	1.62	F606W	—	33.6	2 [†]	0 [†]	1 [†]
NGC 4387	17.9	97.0	0.9	0.6	10.2	2.73	F475W	F850LP	38.7	1	0	1
NGC 4458	16.4	85.0	0.9	0.7	10.0	2.63	F475W	F850LP	34.5	2	0	1
NGC 4550	15.5	110.0	1.3	0.5	10.2	2.60	F475W	F850LP	25.8	6	1	1
NGC 4551	16.1	95.0	1.1	0.7	10.2	2.59	F475W	F850LP	26.6	0	1	0
NGC 7457*	12.9	78.0	2.6	1.4	10.3	5.49	F475W	F850LP	37.7	1	0	2
Total Sample										12	2	6

NOTE.—*Col.(1)*: Target galaxy name. *Col.(2)*: Distance as given by Cappellari et al. (2013). *Col.(3)*: Velocity dispersion from either Halliday et al. (2001) or Cappellari et al. (2006). *Col.(4)* and *(5)*: 2MASS based K -band galaxy major and minor axes from Jarrett et al. (2003). *Col.(6)*: Logarithm of the K -band luminosity. *Col.(7)*: Neutral hydrogen Galactic column density. *Col.(8)* and *(9)*: The available HST imaging (via either ACS or WFPC2 imaging) for “blue” and “red” filters, respectively, which were used to identify and characterize optical counterparts to X-ray sources. *Col.(10)*: Total *Chandra* exposure time. All galaxies were imaged using ACIS-S and had coverage over the entire galactic extents as defined in *Col. (4)* and *(5)*. *Col.(11)–(13)*: The number of field LMXBs (*Col.(11)*), GC LMXBs (*Col.(12)*), and background or central AGN candidates (*Col.(13)*) within the galactic extent of each galaxy (as defined in *Col.(4)* and *(5)*) that had 0.5–7 keV fluxes exceeding that of a $L_X = 10^{38}$ erg s⁻¹ source at the distance provided in *Col.(2)*. X-ray sources were classified using HST data and the procedure outlined in §2.2 of P14.

*Observations of NGC 7457 were represented in both the sample by P14 and this study. However, due to the availability of new HST data for NGC 7457 in this study, results based on our analysis were used throughout this paper.

† For NGC 4339, we considered 74% of the reported K -band luminosity that corresponded to the region of the galaxy covered by the HST WFPC2 footprint detailed in §2. For *Col.(11)–(13)*, we only considered X-ray sources detected in this covered region.

star-formation histories of massive ellipticals would have included early phases of intense starburst activity that produced many massive stars (and a top-heavy IMF), which chemically enriched the galaxies and created turbulence in their interstellar mediums. Subsequent star formation within these environments would be more greatly fragmented and lead to the formation of preferentially smaller stars and bottom-heavy IMFs.

Other authors have taken somewhat different approaches to resolving the above incompatibility issue. Ferreras et al. (2015) focused on the functional form of the IMF and tested a model where the low-mass and high-mass slopes of a broken power law IMF were independently varied. They found that regardless of the IMF slope parameters, a time-independent IMF (independent of galaxy mass) could not simultaneously reproduce the observed chemical enrichment and gravity sensitive spectral features in massive ellipticals. Finally, Martín-Navarro et al. (2014) explored a radial and time-dependent form of the IMF. They argued that in massive ellipticals ($\sigma \approx 300$ km s⁻¹), the radial trends in chemical enrichment and gravity sensitive spectral features could be well described by a time-dependent IMF, like that proposed by Weidner et al. (2013), in the central regions of these galaxies. In contrast, a Milky Way-like IMF was proposed in the galactic outskirts, based on the lack of these spectral signatures relative to the galactic interior. The IMF was then claimed to be a local phenomenon, reflecting a two-stage formation history for these galaxies. Other evidence for radial trends in spectral features follows similar rationales (La Barbera et al. 2016a, 2016b).

The studies above have helped to constrain variations in the low-mass end of the elliptical-galaxy IMF ($\lesssim 0.5 M_\odot$) with galaxy mass but do not place strong constraints on variations of the high-mass end of the IMF. To trace the high-mass end of the IMF requires studying the most massive stars in a galaxy, however these stars evolve quickly into black holes (BHs) and neutron stars (NSs) making them difficult to observe. Fortunately these stellar remnants are found in binary star systems, where a lower-mass and longer-lived companion star eventually becomes a “donor” star, losing mass to the compact object. The system itself radiates nearly all of its energy in the form of X-rays, making these previously undetectable high-mass remnants available to direct observation. Therefore, an efficient and effective way to constrain varia-

tions in the high-mass end of the IMF ($\gtrsim 8 M_\odot$) with galaxy mass is to test for corresponding variations in the prevalence of these low-mass X-ray binary (LMXB) systems in elliptical galaxies. With this in mind, Peacock et al. (2014; hereafter, P14) calculated (using Maraston (2005) population synthesis calculations) that a bottom-heavy single power-law IMF, with $\alpha \approx 2.8$, would yield a factor of ≈ 3 times fewer LMXBs per unit K -band luminosity (N/L_K) over a standard Kroupa (2001) IMF, implying a dramatic decline in N/L_K with increasing σ . Using archival *Chandra X-ray Observatory (Chandra)* and *Hubble Space Telescope (HST)* data of eight nearby elliptical galaxies, P14 found instead that N/L_K was constant with elliptical galaxy luminosity and velocity dispersion; however, their test included only one low-mass elliptical galaxy at $\sigma < 150$ km s⁻¹, where N/L_K was expected to be largest.

In this paper, we augment the P14 study of eight elliptical galaxies by adding *Chandra* constraints for five new low-mass ellipticals ($\sigma = 78$ –110 km s⁻¹) that are predicted to have standard IMFs that differ from those of the massive ellipticals (see, e.g., Cappellari et al. 2012). With this expanded sample of 13 galaxies, we are able to place robust constraints on how N/L_K varies across the full range of velocity dispersion ($\sigma = 80$ –300 km s⁻¹) where significant variations in N/L_K are plausibly expected.

2. SAMPLE AND DATA REDUCTION

Our low-mass elliptical galaxy sample was derived from the samples of Halliday et al. (2001) and Cappellari et al. (2006), which contain velocity dispersion data for several nearby ellipticals. We limited our sample to galaxies with $D < 20$ Mpc, so that we could easily resolve LMXB populations, and $\sigma \lesssim 110$ km s⁻¹, to focus on the galaxies that are likely to have standard IMFs that differ from the already well-studied high-mass ellipticals. In order to guard against potential contamination from young high-mass X-ray binaries (HMXBs), we further restricted our sample to galaxies that had negligible star-formation rate signatures (SFR $< 0.001 M_\odot$ yr⁻¹), as measured by 24 μ m *Spitzer* data (Temi et al. 2009). Our final sample of six low-mass elliptical galaxies is summarized in Table 1.

We conducted new *Chandra* observations for four of the six galaxies to reach 0.5–7 keV point-source detection limits

of $L_X \approx 10^{38}$ erg s^{-1} (chosen for consistency with the sample from P14), after combining with archival *Chandra* data. All observations were conducted using ACIS-S, which covers the entire *K*-band-defined areal footprints of all of the galaxies in our sample (see Table 1 and Jarrett et al. 2003). The only exception was NGC 4339, which only had partial *HST* coverage. For this galaxy, we utilized only the background-subtracted *K*-band flux within the overlapping *HST* footprint, and only LMXBs detected in this region were included in our analyses. This resulted in our using only 74% of the *K*-band luminosity reported in Col.(6) when computing N/L_K for this galaxy.

Data reduction for our sample of galaxies closely follows the procedure outlined in §§2.1 and 2.2 of Lehmer et al. (2013), with our reduction being performed with CIAO v. 4.7 and CALDB v. 4.6.7. We reprocessed events lists from level 1 to level 2 using the script `chandra_repro`, which identifies and removes events from bad pixels and columns, and filters events lists to include only good time intervals without significant flares and non-cosmic ray events corresponding to the standard ASCA grade set (grades 0, 2, 3, 4, 6). For galaxies with more than one observation, we combined events lists using the script `merge_obs`. We constructed images in three X-ray bands: 0.5–2 keV, 2–7 keV, and 0.5–7 keV. Using our 0.5–7 keV images, we utilized `wavdetect` at a false-positive probability threshold of 10^{-5} to create point source catalogs. We converted 0.5–7 keV point-source count-rates to fluxes assuming an absorbed power-law spectrum with a photon index of $\Gamma = 1.5$ and Galactic extinction (see Col. (7) in Table 1). We treated the hot gas component as negligible within the small area of the sources, as these galaxies have very little diffuse emission in total, typical of low-mass ellipticals like those studied here (e.g., O’Sullivan et al. 2001). Our choice of photon index reproduces well the mean 2–7 keV to 0.5–2 keV count-rate ratio of the detected point sources in our sample, a value calculated using stacking analyses (see, e.g., Lehmer et al. 2016 for details).

The total number of sources within each galaxy footprint that had fluxes brighter than the $L_X = 10^{38}$ erg s^{-1} limit span the range of 1–8 (see Col. (11)–(13) of Table 1). Our test of the variation in the IMF with galaxy mass is sensitive to the field LMXB population that forms within the galactic stellar populations. To search for potential contaminants from unrelated X-ray-detected objects, including, e.g., background active galactic nuclei (AGN), foreground Galactic stars, central low-luminosity AGN, and LMXBs formed through dynamical processes in GCs, we made use of archival *HST* data (Col.(8) and (9) in Table 1). Contaminating source populations were identified following the procedure outlined in §2.2 of P14, which makes use of *HST* source colors and morphologies to identify and classify counterparts. Regardless of their nature, we rejected X-ray sources with optical counterparts from further consideration. In total, we rejected 8 of the X-ray sources within the galactic footprints (see Col. (12) and (13) of Table 1) that had optical counterparts, which left 12 candidate field LMXBs with $L_X > 10^{38}$ erg s^{-1} in our sample.

3. RESULTS

In Figure 1(a), we show the number of field LMXBs with $L_X > 10^{38}$ erg s^{-1} per unit *K*-band luminosity, N_{38}/L_K , versus velocity dispersion, σ , for our low-mass ellipticals sample combined with the P14 sample. The “variable” and “invari-

ant” IMF models from P14 are shown in Figure 1(a) with blue and red curves, respectively. The variable model assumes that the IMF makes a transition from Kroupa at $\sigma = 95$ km s^{-1} (i.e., $\log \sigma = 1.98$) to a single power-law with slope $\alpha = 2.8$ at $\sigma = 300$ km s^{-1} (i.e., $\log \sigma = 2.48$; see details below), while the invariant model assumes a Kroupa IMF at all σ .

At first inspection, it seems that the specific frequency of LMXBs indicate that the IMFs of elliptical galaxies are consistent with a single “universal” IMF. However, it is important to note that the LMXB population is tracing only the remnant population from stars with $m \gtrsim 8 M_\odot$. All that can be reliably inferred from the apparent constancy of N_{38}/L_K across σ , is that the single power law slope of the IMF for stars of $m > 0.5 M_\odot$ does not undergo strong variations for ellipticals of all velocity dispersions. In fact, it may be possible that the low-mass end does vary strongly with velocity dispersion, as found in the literature (see references in §1).

With this in mind, we sought to extend P14 by exploring the space of acceptable parameters that could constrain how the IMF might vary, by constructing a suite of IMF models and comparing their predicted N_{38}/L_K versus σ tracks with our constraints shown in Figure 1(a). In this process, we followed a similar, but more generalized procedure to that outlined in §4.2 of P14. Below, we summarize our model.

We began by considering a broken power-law form for an IMF corresponding to high-mass ellipticals:

$$\frac{dN}{dm} = N_0 \begin{cases} 2^{(\alpha_2 - \alpha_1)} m^{-\alpha_1} & 0.1 M_\odot < m < 0.5 M_\odot \\ m^{-\alpha_2} & m > 0.5 M_\odot, \end{cases} \quad (1)$$

where for a Kroupa IMF, $\alpha_1 = 1.3$ and $\alpha_2 = 2.3$. N_0 is a constant of normalization, which, in our procedure, normalizes the 0.1–100 M_\odot integrated IMF to 1 M_\odot . Therefore, N_0 varies with α_1 and α_2 .

Next, we constructed a grid of IMFs over $\alpha_1 = 1-5$ and $\alpha_2 = 1-3.5$ with 801 and 501 steps of 0.005, respectively, thus resulting in a grid of $n = 401,301$ unique IMFs. For the i^{th} IMF, we quantified the *K*-band mass-to-light ratio, $(M/L_K)_i$, by running the stellar population synthesis code PÉGASE (Fioc & Rocca-Volmerange 1997, 1999), adopting for consistency the assumption in P14 of a single burst star-formation history of age 10 Gyr and solar metallicity. In this procedure, M represents the total initial stellar mass and therefore does not vary with age. We defined the ratio of the i^{th} mass-to-light ratio to that of the Kroupa case as

$$R_{(M/L),i} = \frac{(M/L_K)_i}{(M/L_K)_{\text{kro}}} = \frac{L_{K,\text{kro}}}{L_{K,i}}. \quad (2)$$

In order to keep $R_{(M/L)}$ consistent with observations of how the dynamical and stellar M/L varies with σ , we required that $R_{(M/L),i} < 3.0$ (e.g., Cappellari et al. 2012; Conroy et al. 2012). This requirement on $R_{(M/L)}$ resulted in the discarding of models with specific combinations of α_1 and α_2 (notably, models with $\alpha_1 \geq 3.9$ or $\alpha_2 \leq 1.6$ were rejected; see Fig. 1(d)). This constraint limited the number of models considered to $n = 198,298$ total models, which we utilize hereafter.

Because the prevalence of the LMXB population is sensitive to the underlying compact object population of NSs and BHs, which are remnants of $> 8 M_\odot$ stars, we calculated the number of stars per solar mass that become compact objects for a given IMF by integrating the IMF from 8–100 M_\odot :

$$N_{\text{CO},i} = N_{0,i} \int_8^{100} m^{-\alpha_2,i} dm. \quad (3)$$

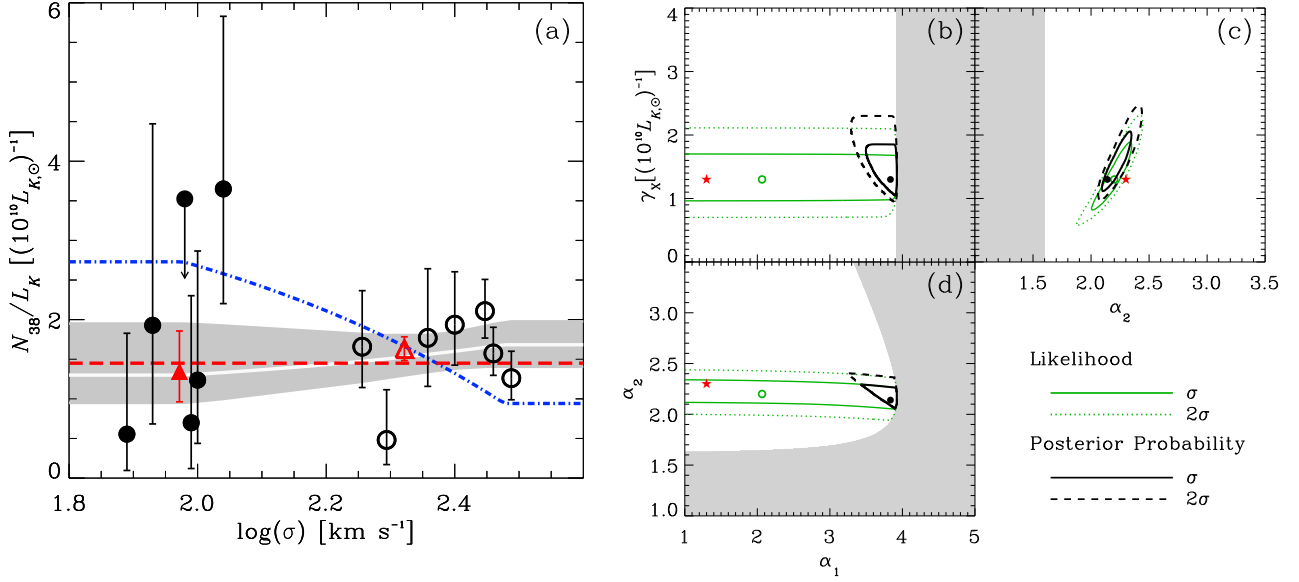


Figure 1. (a) The number of field LMXBs with $L_X \geq 10^{38} \text{ erg s}^{-1}$ per $10^{10} L_{K,\odot}$ versus velocity dispersion, σ , for galaxies from this study (black filled circles) and from P14 (open circles). The red filled triangle represents the mean value from the six galaxies in this study (see Table 1). The red open triangle represents the mean value of the seven high-mass galaxies studied in P14. Error bars are 1σ and were computed following Gehrels (1986). The blue dot-dash curve and red dashed line represent, respectively, the variable and constant IMF scenarios tested by P14. The bold white curve represents our best model with our posterior (see §4) and interpolates between the Kroupa IMF at $\sigma \leq 95 \text{ km s}^{-1}$ to an IMF with $\alpha_1 = 3.84$, $\alpha_2 = 2.14$, and $\gamma_X = 1.30 (10^{10} L_{K,\odot})^{-1}$ at $\sigma \geq 300 \text{ km s}^{-1}$ (see §3 for details). The gray shaded region is our 1σ confidence region about our best model. (b)–(d) Confidence contours for fitting parameters α_1 , α_2 , and γ_X (see §3). The green contours correspond to the likelihood computed using only data from our LMXB study, where the black contours utilize our LMXB data with a prior based on the study by La Barbera et al. (2013; see §4). In each case, the solid and broken (dotted or dashed) curves represent the 1σ and 2σ cuts respectively. The gray shaded region represents the subset of parameter space that is disallowed based on the M/L constraints discussed in §3, which require each model to have an $R_{(M/L),i} < 3.0$. This results in our study discarding $\alpha_1 > 3.9$ and $\alpha_2 < 1.6$, and gives rise to the sharp cut-offs displayed in the contours. Finally, it is important to note that before the application of the prior, α_1 is essentially unconstrained by the broad parameter space that we explored in this study. The green open and black filled points are our best model parameter values before and after the use of the prior, respectively, while the red filled stars are the reference Kroupa values. Values for the best fit before the prior (green open points) are $\alpha_1 = 2.07$, $\alpha_2 = 2.20$, and $\gamma_X = 1.30 (10^{10} L_{K,\odot})^{-1}$; best fit values after the application of the prior (black filled points) are cited above in (a); red filled stars are the Kroupa IMF parameters with $\alpha_1 = 1.3$, $\alpha_2 = 2.3$, and $\gamma_X = 1.30 (10^{10} L_{K,\odot})^{-1}$.

where $N_{0,i}$ is the i^{th} normalization factor. These mass fractions allow us to compute the K -band luminosity normalized ratio of expected NSs and BHs generated by the i^{th} IMF to that of a Kroupa IMF by,

$$R_{\text{CO},i} \equiv \frac{(N_{\text{CO}}/L_K)_i}{(N_{\text{CO}}/L_K)_{\text{kro}}} = \frac{N_{\text{CO},i}}{N_{\text{CO},\text{kro}}} R_{(M/L),i}. \quad (4)$$

From these quantities, we construct a variable IMF model that varies smoothly with σ , bridging the low-mass ellipticals Kroupa IMF to the high-mass ellipticals IMF (i.e., the i^{th} IMF). We define our variable IMF function over the range $\sigma = 95\text{--}300 \text{ km s}^{-1}$, within which we require that the IMF varies as a function of σ following the Cappellari et al. (2013) relation of $(M/L)_\sigma \propto \sigma^{0.72}$. Under these assumptions, we can quantify the fraction of the variable IMF that is composed of the i^{th} IMF as a function of σ to reflect the desired result that galaxies with $\sigma \leq 95 \text{ km s}^{-1}$ have no contribution from the i^{th} IMF, but will only be composed of a Kroupa IMF, while galaxies with $\sigma \geq 300 \text{ km s}^{-1}$ will be solely composed of the i^{th} IMF component:

$$F(\sigma) = \begin{cases} 0 & (\sigma \leq 95 \text{ km s}^{-1}) \\ \frac{\sigma^{0.72} - 95^{0.72}}{300^{0.72} - 95^{0.72}} & (95 \text{ km s}^{-1} < \sigma < 300 \text{ km s}^{-1}) \\ 1 & (\sigma \geq 300 \text{ km s}^{-1}), \end{cases} \quad (5)$$

We define the complementary fraction F_{kro} ,

$$F_{\text{kro}}(\sigma) = 1 - F(\sigma), \quad (6)$$

which is then the fraction of the variable IMF that is composed of a Kroupa IMF.

We combine Equations (4), (5), and (6) and define a composite function:

$$\begin{aligned} R_{\text{comp},i}(\sigma) &\equiv \frac{(N_{\text{CO}}/L_K)_{\sigma,i}}{(N_{\text{CO}}/L_K)_{\text{kro}}} = R_{\text{CO},i}F(\sigma) + F_{\text{kro}}(\sigma) \\ &= 1 - (1 - R_{\text{CO},i})F(\sigma), \end{aligned} \quad (7)$$

which represents the σ -dependent number of compact objects per unit K -band luminosity compared to the Kroupa IMF. We then arrive at a function that can be used to predict the number of observed LMXBs per unit K -band light:

$$\begin{aligned} \left(\frac{N_X}{L_K}\right)_i &= \xi_i \left(\frac{N_{\text{CO},\text{kro}}}{L_{K,\text{kro}}}\right) R_{\text{comp},i}(\sigma) \\ &= \gamma_{X,i} R_{\text{comp},i}(\sigma). \end{aligned} \quad (8)$$

Here ξ_i represents the luminosity-dependent fraction of the compact object population that is actively involved in an LMXB phase, derived using the i^{th} model. $\gamma_{X,i}$ is a fitted scaling factor for the i^{th} model that allows us to express this quantity as an observed frequency of LMXBs by correcting for a

portion of N_{CO} which are not LMXBs (e.g. BH-BH pairs, BH-NS pairs, etc.). We note that we assume that ξ is independent of σ , which simplifies the computation of our IMF models, but may not be physically accurate. A more detailed treatment requires X-ray binary population synthesis modeling for various IMFs (e.g., Fragos et al. 2013), that would involve variations in the mass ratio distribution with IMF. However, such treatments are likely to introduce many parameters into the analysis for which there are no plausible physical models for varying binarity, and for which there are no solid empirical constraints, making the benefit of such modeling inconclusive. Such work is beyond the scope of this paper (see §4).

Using Equation (8), and the constraints on N_{38}/L_K presented in Figure 1(a), we computed maximum likelihood values for all 198,298 IMFs in our grid using the Cash statistic (cstat; Cash 1979). This procedure resulted in a normalized likelihood cube with three dimensions: α_1 , α_2 , and γ_X . From our grid of models, the maximum-likelihood model and 1σ errors are $\alpha_1 = 2.07^{+1.9}_{-1.1}$, $\alpha_2 = 2.20^{+0.17}_{-0.24}$, and $\gamma_X = 1.30^{+0.55}_{-0.45} (10^{10} L_{K,\odot})^{-1}$ (see the 68% and 95% green contours in Fig. 1(b)–1(d)).

As we suspected, LMXBs provide stringent constraints on variations of the IMF for intermediate to massive stars (i.e., $m > 8 M_\odot$), and to the extent that we assume a single power law over the range of $m > 0.5 M_\odot$, a stringent constraint on α_2 . However, LMXBs essentially provide no useful constraints on the low-mass IMF slope.

Indeed, in Figure 1(a) we can surmise that the “invariant” case (red curve) is formally acceptable and within the 1σ threshold of our maximum probability model, while the interpolation to a single power-law IMF with $\alpha = 2.8$ (blue curve) is not consistent with the LMXB observations. With an enhanced galaxy sample we not only confirm the result of P14 with better statistics, but also extend it by showing that it is possible to have an IMF that varies from being Kroupa for low-mass ellipticals to being bottom-heavy for high-mass ellipticals, as has been reported in the literature. In addition, the LMXB data suggest that the single power law slope for such a varying IMF above $0.5 M_\odot$ is unlikely to change much with velocity dispersion. In the next section, we utilize the formalism above, combined with a prior on how the IMF mass fraction due to low-mass stars can vary with velocity dispersion, to better constrain the values of α_1 , α_2 , and γ_X .

4. DISCUSSION AND CONCLUSIONS

As discussed in §3, LMXBs provide strong constraints on the variation of the IMF for stars with $m > 0.5 M_\odot$ with velocity dispersion; however, variations in the low-mass end of the IMF are not well constrained by LMXBs alone. The green contours in Figure 1(b)–1(d) show our 1 and 2σ confidence intervals for α_1 , α_2 , and γ_X using only LMXB data.

It is clear that these data are unable to constrain well α_1 ; however, we show that the model slope above $0.5 M_\odot$, α_2 , and normalization factor γ_X , were strongly constrained. In order to better constrain α_1 , we utilized a prior derived by La Barbera et al. (2013), who concluded that the gravity-sensitive near-IR absorption features observed in high-mass elliptical galaxy ($\sigma \approx 300 \text{ km s}^{-1}$) spectra require ≈ 70 – 90% of the total initial stellar mass to be contained in stars with $m < 0.5 M_\odot$, as integrated directly from the IMF. From Equation (1), we can compute the low-mass fraction for each of the n IMF mod-

els defined above following

$$\begin{aligned} f_i(< 0.5 M_\odot) &= \frac{M(< 0.5 M_\odot)_i}{M_\odot} \\ &= \frac{N_{0,i} 2^{\alpha_{2,i} - \alpha_{1,i}}}{M_\odot} \int_{0.1}^{0.5} m^{-\alpha_{1,i} + 1} dm. \end{aligned} \quad (9)$$

Using the low-mass fractions calculated via Equation (9), we next assigned a flat prior of 1 for $0.7 < f_i < 0.9$, and 0 elsewhere for our grid of IMF models. Multiplying this prior by our likelihood cube (see §3), and renormalizing, resulted in a posterior probability distribution which we display as black contours in Figure 1(b)–1(d). The resulting posterior probability provides a stringent constraint on α_1 for massive ellipticals, resulting in best model values of $\alpha_1 = 3.84^{+0.09}_{-0.48}$, $\alpha_2 = 2.14^{+0.20}_{-0.85}$, and $\gamma_X = 1.30^{+0.65}_{-0.35} (10^{10} L_{K,\odot})^{-1}$. The white curve, and gray 1σ envelope, displayed in Figure 1(a) shows our best model, which smoothly varies between a Kroupa IMF for low-mass ellipticals, to a broken power-law IMF for high-mass ellipticals. The high-mass galaxy IMF component has a steep slope of $\alpha_1 = 3.84$ for stars $< 0.5 M_\odot$, and a slope of $\alpha_2 = 2.14$ for stars $\geq 0.5 M_\odot$. We note that while α_2 is slightly flatter than the slope given by Kroupa, it still squarely falls within the uncertainty of the Kroupa IMF ($\alpha_2 = 2.3 \pm 0.7$; Kroupa, 2001).

By construction, this result is consistent with both the IMF for massive ellipticals being bottom-heavy, as inferred in the literature (see references in §1), and the IMF not varying significantly across the mass spectrum at the high-mass end, as inferred by the LMXB populations (see also P14). Additionally, the variable IMF has been constructed to yield a total (including stellar remnants) mass-to-light ratio that varies with velocity dispersion following the observational constraints from Cappellari et al. 2013. In absolute terms, the stellar mass-to-light ratio of our best-fit model, varies from $M_*/L_K = 0.679$ at $\sigma = 90 \text{ km s}^{-1}$ to $M_*/L_K = 3.10$ at $\sigma = 300 \text{ km s}^{-1}$. The initial mass-to-light ratios, (initial stellar mass over K -band luminosity) are $M/L_K = 1.48$ at $\sigma = 90 \text{ km s}^{-1}$ to $M/L_K = 4.12$ at $\sigma = 300 \text{ km s}^{-1}$, resulting in a ratio $R_{M/L} = 2.78$. These values are below the limits placed on the dynamical mass-to-light ratio values measured in the literature (e.g., Cappellari et al. 2013; Conroy et al. 2013).

We also noted in §1 that recent studies have found evidence for radial gradients in the IMFs of massive ellipticals, in which a bottom-heavy IMF appears to be appropriate for the inner regions of the galaxy, while a more Kroupa-like IMF is appropriate in the outer regions (see, e.g., Martín-Navarro et al. 2015; La Barbera et al. 2016a, 2016b). We tested to see whether the LMXB population showed evidence for such radial gradients by calculating the average N_{38}/L_K values for LMXBs that were located within and outside of the effective radii, r_e , of the massive elliptical galaxy population. We utilized r_e values from Cappellari et al. (2013) to divide the $L_X > 10^{38} \text{ erg s}^{-1}$ LMXB catalogs from Peacock et al. (2014) into inner- and outer-LMXB populations, and used the 2MASS K -band images to calculate the fraction of L_K that was within and outside of r_e . We found consistent values of $N_{38}/L_K = 1.4 \pm 0.5$ and 1.7 ± 0.6 for the regions within and outside r_e , respectively, indicating that such gradients do not have a significant effect on our results.

To emphasize, our likelihoods are broadly insensitive to α_1 . We relied on La Barbera et al. (2013) as a meaningful prior and showed we are able to reconcile their results with our

analysis, with a statistically insignificant change in the derived values for the other two parameters, α_2 and γ_X . A choice of a different, meaningful prior would necessarily entail a different posterior probability density for α_1 , however, the essential constraint that this study places on α_2 would not change significantly.

If a slight flattening of the high-mass slope of the generalized IMF is common in high-mass elliptical galaxies (shown to be required if we accept that the bottom-heavy IMF claims in the literature are correct), then several additional predictions result. We would expect a factor of ~ 2 higher supernova rate in the high redshift versions of these galaxies than their present day stellar masses imply. A more severe effect might be seen on the rate of long duration gamma-ray bursts (GRBs), which are often thought to come from only the most massive stellar explosions. Presently, we have limited information about very high-redshift GRBs, and almost no information about very high-redshift supernovae (SNe). The information that exists suggests a GRB rate not easily explained by detectable star forming galaxies (Tanvir et al. 2012), but the present results are easily explained by having most of the star formation take place in relatively small galaxies, below the *HST* detection threshold. We would expect similar increases in the rates of double neutron star mergers producing short GRBs and gravitational wave sources, as well as an enhancement, albeit a somewhat lower one, of the rate of Type Ia SNe, since more white dwarfs would be produced and they would be skewed more heavily toward the massive end of the white dwarf spectrum.

It is also important to note that if the slope of the high-mass end of the IMF changes by about 0.1 dex, then the ratio of core collapse supernovae from $\approx 40 M_\odot$ stars to that from $\approx 8 M_\odot$ stars changes by a factor of about 20%. The yields from the most massive core collapse supernovae to those from the least massive ones can vary quite dramatically (e.g. Kobayashi et al. 2006). As a result, interstellar medium abundances may provide a complementary test of the IMF. Because additional metal enrichment comes from thermonuclear supernovae, classical novae, and mass loss, a detailed treatment of this problem must be undertaken before a clear prediction can be made.

Future X-ray and high-resolution optical observations, and new population synthesis analyses could substantially improve constraints on the IMF variation with velocity dispersion. In particular, new *Chandra* and *HST* observations of low-to-intermediate mass ellipticals would be helpful in ruling-out a scenario where the high-mass end of the IMF is constant across all σ . Deeper *Chandra* observations of the low-mass galaxies in this study would have a similar effect, allowing us to probe to the more numerous population of low-luminosity LMXBs. In a forthcoming paper, Peacock et al. (in-prep), will be examining the $L_X \gtrsim 10^{37}$ erg s⁻¹ field LMXB population in low-mass elliptical NGC 7457 and comparing it with similar binaries detected in deep observations of massive ellipticals.

Most effectively testing the variations of the IMF in elliptical galaxies will require simultaneous modeling of near-IR spectroscopic data along with LMXB constraints using the combination of stellar population synthesis and X-ray binary population synthesis modeling (e.g., Fragos et al. 2013; Madau & Fragos 2016), in which the IMF, stellar ages, metallicities, and other physical parameters that influence X-ray binary formation are all modeled self-consistently. Such a pop-

ulation synthesis framework will be an important future step for advancing our knowledge of how the IMF varies among elliptical galaxies.

Additionally, a further understanding of the details of the stellar populations in the near-IR must be developed to ensure that the claims of a bottom-heavy IMF are reliable. At the present time, stellar evolution codes used for these purposes have limited or no treatment of unusual classes of stars such as interacting binaries and the products of binary interactions. Such stars are likely to be relatively unimportant for tracing out the optical bands where the models have been best calibrated, however, given that the largest radius stars are most likely to interact, these stars may be increasingly important toward the reddest parts of the spectral energy distribution where red giants and asymptotic giant branch stars are most important. For instance, it has already been shown that the S-type stars might appear with different frequencies in larger and smaller elliptical galaxies, and can potentially mimic the effects of bottom-heavy IMFs on the Wing-Ford band and the Na I D line, although not on Ca II (Maccarone 2014).

Given the coincidence needed between changes in both the high- and low-mass ends of the IMF to reproduce the results we see here, as well as the subtlety of the features that have been used to suggest the bottom-heavy IMF, more work to investigate further the level of systematic effects from stars not included in standard stellar population synthesis models would be well-motivated.

D.A.C., B.D.L., and R.T.E. gratefully acknowledge support from *Chandra* X-ray Center (CXC) grant GO4-15090A. D.A.C. acknowledges support from USRA and GSFC, as well as generous support from the University of Arkansas. A.K. acknowledges CXC grants GO4-15090C and GO5-16084B, and T.M. acknowledges GO4-15090B. M.P. and S.Z. acknowledge support from NASA ADAP grant NNX15AI71G, and M.P. additionally acknowledges CXC grant GO5-16084A and the *Hubble Space Telescope (HST)* grant HST-GO-13942.001-A.

REFERENCES

- Auger, M. W., Treu, T., Bolton, A. S., et al. 2010, *ApJ*, 724, 511
 Bastian, N., Covey, K. R., & Meyer, M. R. 2010, *ARA&A*, 48, 339
 Cappellari, M., McDermid, R. M., Alatalo, K., et al. 2012, *Nature*, 484, 485
 Cappellari, M., Scott, N., Alatalo, K., et al. 2013, *MNRAS*, 432, 1709
 Cash, W. 1979, *ApJ*, 228, 93
 Cenarro, A. J., Gorgas, J., Vazdekis, A., Cardiel, N., & Peletier, R. F. 2003, *MNRAS*, 339, L12
 Chabrier, G. 2003, *PASP*, 115, 763
 Conroy, C., & van Dokkum, P. G. 2012, *ApJ*, 760, 71
 Conroy, C., Dutton, A. A., Graves, G. J., Mendel, J. T., & van Dokkum, P. G. 2013, *ApJL*, 776, L26
 Ferreras, I., Weidner, C., Vazdekis, A., & La Barbera, F. 2015, *MNRAS*, 448, L82
 Fragos, T., Lehmer, B., Tremmel, M., et al. 2013, *ApJ*, 764, 41
 Gehrels, N. 1986, *ApJ*, 303, 336
 Hardy, E., & Couture, J. 1988, *ApJL*, 325, L29
 Kroupa, P. 2001, *MNRAS*, 322, 231
 La Barbera, F., Ferreras, I., Vazdekis, A., et al. 2013, *MNRAS*, 433, 3017
 La Barbera, F., Vazdekis, A., Ferreras, I., Pasquali, A., Cappellari, M., Martín-Navarro, I., Schönebeck, F., Falcón-Barroso, J. 2016a, *MNRAS*, 457, 1648
 La Barbera, F., Vazdekis, A., Ferreras, I., Pasquali, A., Allende Prieto, C., Rock, B., Aguado, D. S., Peletier, R. F. 2016b, arXiv:1610.03853
 Lehmer, B. D., Basu-Zych, A. R., Mineo, S., et al. 2016, *ApJ*, 825, 7
 Maccarone, T. J. 2014, *MNRAS*, 442, L5
 Madau, P., & Fragos, T. 2016, arXiv:1606.07887
 Maraston, C. 2005, *MNRAS*, 362, 799

- Martín-Navarro, I., La Barbera, F., Vazdekis, A., Falcón-Barroso, F., Ferreras, I. 2015, *MNRAS*, 477, 1033
- Miller, G. E., & Scalo, J. M. 1979, *ApJS*, 41, 513
- Offner, S. S. R., Clark, P. C., Hennebelle, P., Bastian, N., et al. 2014, *Protostars and Planets VI*, 914, 53
- O'Sullivan, E., Forbes, D. A., Ponman, T. J. 2001, *MNRAS*, 328, 461
- Peacock, M. B., Zepf, S. E., Maccarone, T. J., et al. 2014, *ApJ*, 784, 162
- Saglia, R. P., Maraston, C., Thomas, D., Bender, R., Colless, M. 2002, *ApJ*, 121, 161
- Salpeter, E. E. 1955, *ApJ*, 121, 161
- Shapiro, K. L., et al. 2010, *MNRAS*, 402, 2140
- Smith, R. J., Lucey, J. R. 2013, *MNRAS*, 434, 1964
- Smith, R. J. 2014, *MNRAS*, 443, 69
- Tanvir, N. R., Levan, A. J., Fruchter, A. S., et al. 2012 *ApJ*, 754, 46
- Treu, T. 2010, *ARA&A*, 48, 87
- van Dokkum, P. G., & Conroy, C. 2010, *Nature*, 468, 940
- van Dokkum, P. G., & Conroy, C. 2011, *ApJL*, 735, L13
- van Dokkum, P. G., & Conroy, C. 2012, *ApJ*, 760, 70
- Weidner, C., Ferreras, I., Vazdekis, A., & La Barbera, F. 2013, *MNRAS*, 435, 2274